An Interaction between Moringa Oleifera Biosurfactant and Nanoparticles for Foam Stability, Interfacial Tension Reduction and Wettability Alteration

Umar Hassan, Bayero University Kano, Kano, Nigeria; **Mohammed Falalu Hamza***, Bayero University Kano, Kano, Nigeria and Universiti Teknologi MARA, Selangor, Malaysia; **Hassan Soleimani**, Universiti Teknologi PETRONAS, Perak Darul Ridzuan, Malaysia; **Bashir Abubakar Abdulkadi**r, Universiti Malaysia Pahang Al-Sultan Abdullah, Pahang, Malaysia and Gombe State University, Gombe, Nigeria; **Saifullahi Shehu Imam**, Bayero University Kano, Kano, Nigeria; and **Sabiha Hanim Saleh**, Universiti Teknologi MARA, Selangor, Malaysia

Abstract

Foam has emerged as one of the most advanced techniques to address the gas mobility challenges encountered during gas flooding in oil reservoirs. Due to environmental concerns, bio-surfactants derived from plants are increasingly recommended as alternatives to synthetic surfactants. This study focuses on synthesizing a Moringa oleifera biosurfactant (MS) reinforced with Silica nanoparticles (SNPs) to produce a nano-foam (MS/SNPs). Adsorption isotherm studies, including the Langmuir and Freundlich models, were utilized to investigate the adsorption of MS onto SNPs. Additionally, the physicochemical properties of the MS/SNPs foam, such as bubble size, foamability, foam stability, interfacial tension (IFT), and contact angle (CA), were thoroughly examined.

The results indicate that the MS synthesis was successful, with significant adsorption capacity onto SNPs. The maximum adsorption was achieved with 4 wt% MS and 0.4 wt% SNPs at 50°C and pH 9, fitting well with the Freundlich isotherm model, showing an R^2 value of 0.9725. According to the Ross-Miles foam test, MS exhibited greater foamability and stability, albeit with lower morphological quality compared to MS/SNPs. Notably, MS/SNPs reduced the IFT of the oil/brine system from 6.22 mN/m to a remarkably low 0.08 mN/m. Moreover, MS/SNPs altered the rock/oil wettability by 24%, favoring more wettable conditions.

Introduction

Crude oil remains a predominant energy source and continues to play a crucial role in addressing global energy demands (Hamza et al. 2018). Projections indicate that global energy demand will increase by 30% by 2040, with oil consumption expected to rise from approximately 87 million barrels per day (Mbpd) in 2010 to over 100 Mbpd (Ahmadi and Shadizadeh 2013; Zhang et al. 2020). Petroleum reservoirs contain significant quantities of hydrocarbons entrapped within porous rock formations (Aljuboori et al. 2019; Hamza et al. 2020). Given the depletion of conventional oil resources, coupled with rising energy demands, population growth, and rapid industrialization, there is an urgent need to enhance oil recovery from existing reserves (Joshi et al. 2015).

Improved Oil and Gas Recovery

DOI: 10.14800/IOGR.1302

Received August 1, 2024; revised August 14, 2024; accepted August 21, 2024.

*Corresponding author: hamzafalal84@gmail.com

Oil recovery is typically categorized into three stages: primary, secondary, and tertiary, the latter often referred to as Enhanced Oil Recovery (EOR). Primary recovery relies on the natural drive mechanisms of the reservoir, while secondary recovery employs water injection to maintain reservoir pressure. However, these methods generally recover less than 30% of the original oil in place (OOIP), leaving a substantial portion of hydrocarbons trapped due to factors such as wettability, capillary forces, and interfacial tension between the reservoir fluids and rock matrix (Hamza et al. 2016).

To maximize hydrocarbon extraction, EOR techniques are employed once primary and secondary methods become ineffective. EOR processes involve the introduction of external agents or energy to modify the physical and chemical interactions within the reservoir, thereby enhancing oil displacement (Osama and Ahmad 2020). Extensive research has been conducted on various EOR techniques, which are categorized based on the nature of the agents used or the mechanisms they invoke (Alireza and Delshad 2023). **Figure 1** illustrates a schematic of EOR methods, highlighting the diverse chemical agents employed.

Chemical Enhanced Oil Recovery (CEOR) is particularly noteworthy due to its ability to alter wettability and reduce interfacial tension, thereby mobilizing trapped oil (Hamza et al. 2018). CEOR involves the injection of chemical solutions, such as alkalis, surfactants, nanoparticles (NPs), and polymers, into the reservoir to improve oil recovery efficiency (Salehi et al. 2014). These chemical agents interact with the oil/water/rock system to overcome the forces that trap oil, facilitating its movement toward production wells and ultimately enhancing recovery rates.

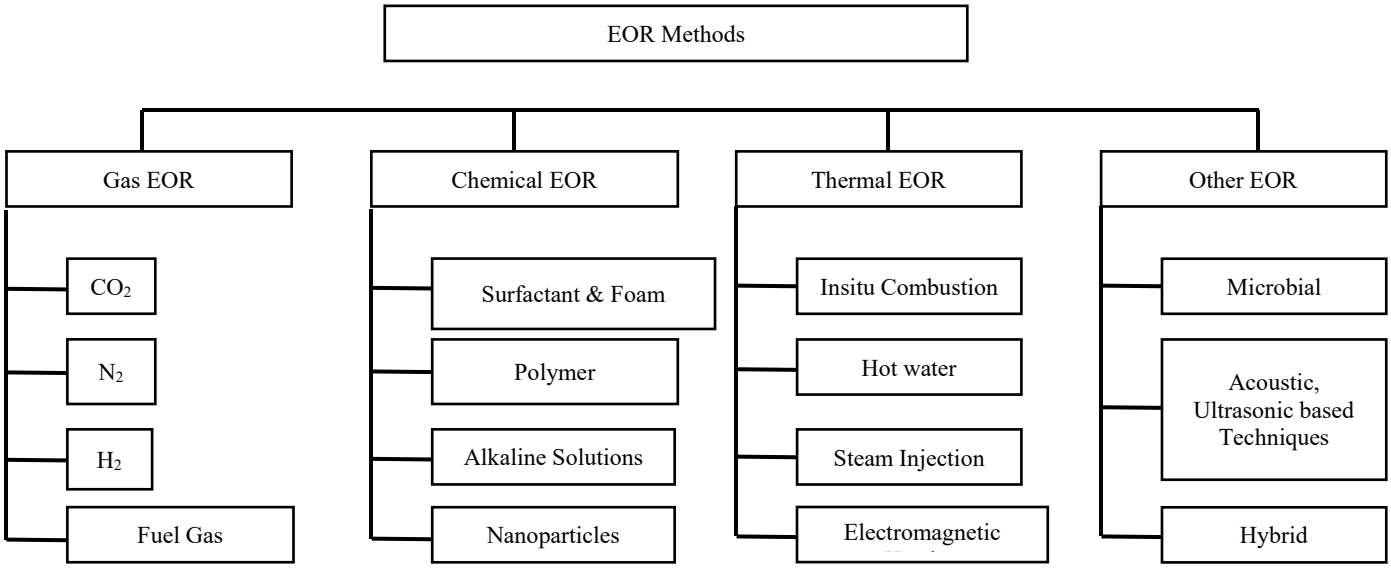

Figure 1—Classification of EOR methods.

Surfactants play significant roles in most CEOR systems, including surfactant flooding, polymer-surfactant flooding, and foam flooding (Blaker et al. 2002). The primary advantage of surfactant-based systems lies in their ability to reduce interfacial tension (IFT) and, in some cases, control gas mobility (Hou et al. 2012; Hamza et al. 2017). However, the effectiveness of surfactants is often compromised by harsh reservoir conditions, such as high temperature, pressure, salinity, and the specific characteristics of the crude oil. Under these circumstances, surfactant flooding alone may not achieve optimal oil recovery (Zhao et al. 2015).

To address these limitations, CEOR strategies involving hybrid materials-such as surfactant-polymer, polymer-nanomaterial, surfactant-nanomaterial, or polymer-surfactant-nanomaterial combinations-have been developed. The synergistic interaction between these hybrid components enhances the rheological properties of the system, improves thermal and salinity resistance, and enables the CEOR hybrids to better withstand variations in crude oil properties (Kamal et al. 2017). In recent years, there has been a growing interest in the

application of nanoparticles (NPs) in conjunction with surfactants to mitigate the challenges associated with surfactant-based EOR processes. This interest is driven by the potential benefits of surface-active complexes formed through electrostatic interactions between NPs and surfactant molecules (Yekeen et al. 2019).

Previous studies have demonstrated the successful generation and propagation of nanoparticle-stabilized foams in the presence of oil (Nguyen et al. 2014). Notably, NPs have been explored as a means of reducing IFT in porous media. For example, hydrophilic NPs dispersed in brine have been shown to reduce IFT from 14.7 to 9.3 mN/m. Dispersing ZnO in brine led to an IFT reduction from 13.38 to 11.60 mN/m, while Fe_2O_3 dispersed in propanol reduced IFT from 38.50 to 2.75 mN/m. Similarly, Al_2O_3 dispersed in propanol lowered IFT from 38.50 to 2.25 mN/m. Furthermore, increasing the concentration of hydrophilic NPs from 0.01 to 0.05 wt.% resulted in a further IFT reduction from 9.3 to 5.2 mN/m (Hassan et al. 2021; Yarima et al. 2022; Hamza et al. 2022).

Atta et al. (2020) reviewed the advantages of NPs as foam stabilizers, highlighting their ability to enhance foam stability under reservoir conditions. This improvement is attributed to the irreversible adsorption and accumulation of NPs at the plateau boundaries and gas-liquid interfaces, which limits fluid-fluid contact, hinders gas diffusion, and reduces liquid drainage (Hamza et al. 2017).

Natural surfactants offer advantages such as high biodegradability, low toxicity, multifunctionality, environmental compatibility, and broad availability, making them suitable for a variety of EOR applications (Ummusalma and Hamza, 2022). These surfactants are typically derived from plant-based materials, including the stem bark, seeds, roots, and leaves.

Moringa oleifera (MO) is a plant native to India, commonly found in tropical and subtropical regions worldwide (Kalibbala et al. 2009) (**Figure 2a**). Known as the "horseradish tree" or "drumstick tree," MO is highly resilient, capable of withstanding both moderate frost and severe drought, and is thus cultivated globally. Due to its high nutritional content, every part of the tree is valuable for both nutritional and commercial applications (Asante et al. 2014; Lakshmipriya et al. 2016; Oyeyinka et al. 2018). The leaves are rich in minerals, vitamins, and phytochemicals, and have been used to treat malnutrition and enhance breast milk production in nursing mothers. MO also exhibits antimicrobial, antidiabetic, anticancer, anti-inflammatory, and antioxidant properties. The seeds (**Figure 2b**), widely utilized in industrial applications and water treatment as a natural coagulant, contain oils and essential fatty acids that can be extracted using solvents such as n-hexane, chloroform, diethyl ether, acetone, and ethanol (Ali et al. 2017; Emilianny et al. 2021). The oil, as illustrated in **Figure 2c**, is rich in various beneficial components, including fatty acids.

(a) Plant (b) Seeds (c) Component distributions

Figure 2—Moringa oleifera.

Methodology

Sample Collection and Pre-treatment. Mature seeds of Moringa oleifera were sourced from Rano Local Government, Kano State, Nigeria. The plant species was authenticated at the Herbarium Research Laboratory, Bayero University Kano, Nigeria. Following authentication, the seeds were dehulled, thoroughly cleaned, and

air-dried for three days. The dried seeds were then mechanically ground to a uniform particle size of 2 mm using a manual grinder. The ground sample was further dried in an oven at 30 °C for 30 minutes to remove any residual moisture.

Determination of Moisture Content. To determine the moisture content, the sample was weighed before and after oven drying. The initial and final masses were recorded, and the moisture content was calculated as a percentage based on the difference between the initial and final masses, as expressed by **Eq. 1**.

$$\text{Moisture content (\%)} = \frac{M1-M2}{M2} \times 100, \quad (1)$$

where, M_1 and M_2 are initial and final masses in g, respectively.

Determination of Acid Value. A precisely weighed 10.2 g sample was dissolved in 0.1 N alcoholic potassium hydroxide (KOH) within a titration vessel. The solution was then titrated potentiometrically. The titration data, consisting of the potentiometric readings and corresponding volumes of titrant, were plotted to generate a titration curve. The end points were identified at distinct inflection points on the curve, and the acid value (in mg KOH/g) were calculated using **Eq. 2**.

$$\text{Acid value} = (A-B) \times M \times \frac{56.1}{W}, \quad (2)$$

Where A is the sample titration volume of alcoholic KOH solution used, mL ; B represents the volume corresponding to A for blank titration, mL; M is concentration of alcoholic KOH solution, mol/L; W is a sample mass, g.

Determination of Saponification Value. A precisely weighed seed sample of 2g was placed into a flask containing 25mL of a solution composed of equal volumes of ethanol and potassium hydroxide (KOH). The flask was connected to a reflux condenser via a Soxhlet extractor and placed in a water bath, maintaining a temperature of 60 to 70^{o}C for 30 minutes with continuous stirring. After the reaction, a few drops of phenolphthalein indicator were added to the extract, which was then titrated against 0.5N hydrochloric acid (HCl). A control experiment was conducted by repeating the entire procedure without the seed sample, serving as a blank. The saponification value was calculated using **Eq. 3**.

$$\text{Saponification value} = \frac{(B-S)\times N\times 56.1}{m}, \quad (3)$$

where, B is the volume of titre blank, mL; S is the volume of titre value with sample, mL; N represents normality of titrating solution (KOH used herein), eq/L; m is the mass of sample, g.

Extraction and Synthesis. A sample of 30 g of prepared Moringa oleifera seeds was placed into a Soxhlet extractor, followed by the addition of 300 ml of ethanol. The extraction was conducted at 60-65°C, just below the boiling point of ethanol, and was repeated for approximately 9 reflux cycles over 3 hours. The resulting mixture of solvent and extracted oil was allowed to settle in a desiccator for 3 days until the solvent was fully evaporated. The purified oil extract was treated with diethyl ether and then left to air dry, eliminating any residual solvent odor. The oil yield was calculated as the ratio of the mass of extracted oil to the initial mass of the seed sample, expressed as a percentage.

For the synthesis of Moringa oleifera surfactant (MS), 20ml of extracted moringa oil was heated to 80-90°C for 30 minutes to simmer the oil. Subsequently, 10g of NaOH was added, and the mixture was maintained at 80°C for approximately 3 hours until a dark solid product formed. To confirm the completion of the reaction, a small portion of the solid was dissolved in distilled water, yielding a clear, uniform solution, as depicted in **Figure 3**.

FTIR Analysis. The solid product was analyzed using Fourier Transform Infrared Spectroscopy (FTIR) with a PerkinElmer Spectrum spectrometer to study its chemical properties by comparing its spectral absorptions with those of the extracted oil. A small amount of the solid sample was placed in the FTIR spectrometer, where the absorption range was measured between 200 and 4000 cm^{-1}. The transmittance was recorded against the wave number, allowing for the identification and characterization of functional groups within the sample.

Figure 3—Synthesis of surfactant.

Formulation Optimization. ***Optimization of MS Adsorption onto SNPs***. To determine the optimal concentration of Moringa oleifera surfactant (MS) adsorbed onto silica nanoparticles (SNPs), MS was prepared at various concentrations ranging from 1 to 5 wt%, with each solution containing a fixed SNPs concentration of 0.2 wt% (**Figure 4**). The SNPs were dispersed in 0.3 wt% brine. The mixtures were agitated on an orbital shaker at 300 rpm for 60 minutes at a controlled temperature of 37 °C. After agitation, the mixtures were filtered through Whatman filter paper. The filtrates were then analyzed using a UV spectrophotometer to determine the concentration of MS remaining in solution. The adsorption of MS onto SNPs at equilibrium was calculated using **Eq. 4**,

$$\text{Adsorption (\%)} = \frac{(C_i - C_f) \times V}{W} \times 100 \quad \text{.....(4)}$$

where C_i is initial concentration of surfactant, wt% or mg/L; C_f is final concentration of surfactant, wt% or mg/L; V is volume of MS/SNPs mixture used, mL; W is weight of SNPs, g.

Figure 4—Optimization of MS concentration.

Optimization of SNPs Dosage. To determine the optimum dosage of silica NPs (SNPs) for maximum adsorption, various concentrations of SNPs ranging from 0.1 to 0.5 wt% (**Figure 5**) were prepared. Each concentration contained a fixed amount of Moringa oleifera surfactant (MS) at the previously determined optimum concentration, which was 4wt% after observing adsorption behaviour with initially a fixed low

concentration of 1wt% of MS. The mixtures were agitated for 60 minutes at 300 rpm and 37°C. Following agitation, the mixtures were filtered, and the filtrates were analyzed using a UV spectrophotometer to assess the concentration of MS remaining in solution.

Figure 5—Optimization of SNPs dosage.

Optimization of Contact Time. For optimizing contact time, the fixed concentrations of MS (4 wt%) and SNPs (0.4 wt%) were used. The mixtures were agitated for varying periods of 30, 60, 90, 120, and 150 minutes (**Figure 6**). After the specified agitation times, the mixtures were separated by filtration, and the filtrates were analyzed using a UV-visible spectrophotometer to determine the adsorption efficiency at each time interval.

Figure 6—Contact time optimization of MS/SNPs.

Effect of Temperature and pH on Optimized Formulation. After establishing the optimized conditions for concentration, dosage, and contact time, the effect of temperature on the formulation was evaluated. The mixture was heated to various temperatures of 20, 30, 40, 50, and 60 °C while maintaining constant shaking at 300 rpm. The samples were analyzed to determine the impact of temperature on the adsorption efficiency.

To determine the optimum pH, the initial pH of the mixture (9.41) was adjusted to different values (2, 5, 7, 9, and 11) using 0.5N HCl and 0.5N NaOH. A pH meter was used to achieve accurate pH adjustments. The resulting mixtures at these different pH levels were then analyzed using a UV spectrophotometer to assess the impact of pH on the adsorption process.

Foam Studies. The Ross-Miles method, as illustrated in **Figure 7**, was employed to evaluate the foamability and stability of Moringa oleifera surfactant (MS) and the MS/Silica Nanoparticles (SNPs) formulation under optimized conditions (Ummusalma and Hamza 2023). For each solution, precisely 5 mL was transferred into a standardized burette (75 × 1.5 cm). The solution was then allowed to flow through the tap into a receiver vessel (measuring cylinder) positioned 9.5 cm below the tap. The turbulence generated during this process resulted in foam bubble formation. The maximum foam height was measured immediately after foam generation, and the half-life of the foam ($t_{1/2}$) was recorded to assess the rate of foam degradation. Foam height measurements were

taken above the water gradient, and it was crucial to maintain a constant distance between the burette and the measuring cylinder throughout the experiment. Foamability and stability were determined based on average foam heights and stabilities, with each experiment being conducted in duplicate for accuracy. In addition, the MS/SNPs solution was prepared in brine (0.3%) and subjected to foamability and stability studies using the Ross-Miles method.

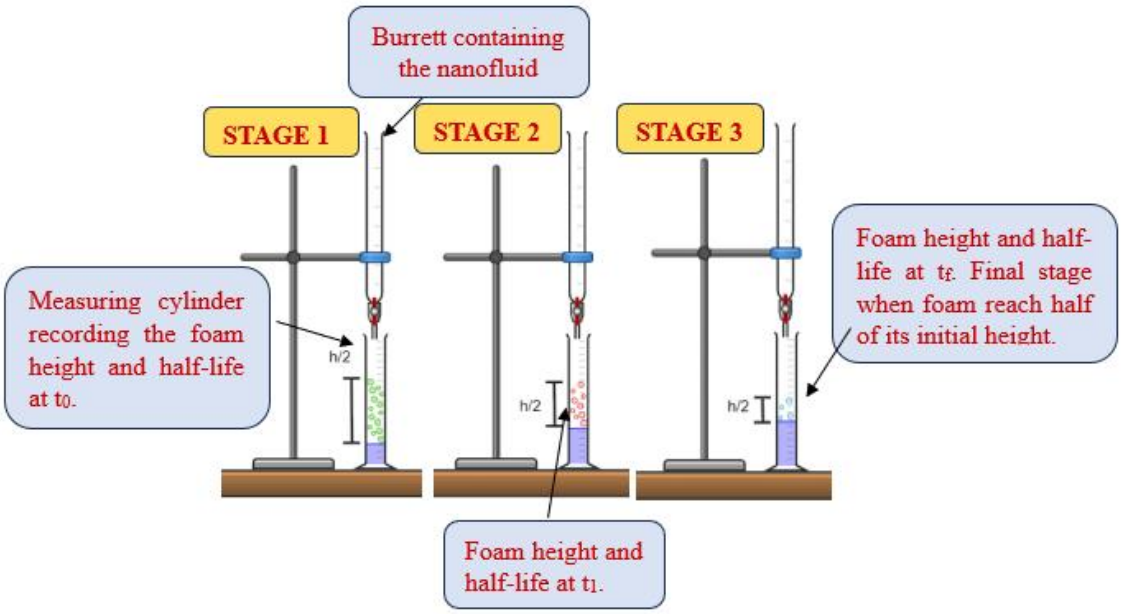

Figure 7—Illustration of Ross mile method.

Foam Morphology Analysis. The foam morphology is made up of the bubble size and distribution. Using a high-resolution KERN transmitted light microscope (OBF-1), the foam microstructure was examined. In order to examine the bubble coalescence, changes in the size and dispersion of the bubbles were tracked at three different time intervals: 0, 5, and 10 minutes. The foam microscopic morphology was measured and captured on camera.

Interfacial Tension (IFT) Measurement. The interfacial tension (IFT) was measured using a spinning drop apparatus (SVT20) at a temperature of 80°C and a rotational speed of 4000 rpm. The formulation of pure MS, MS/SNPs at optimum condition and Brine baseline were prepared as shown in **Figure 8a.** The IFT between crude oil and brine systems was recorded to establish a baseline IFT (Freer et al. 2003).. The procedure involved the following steps:

1. The IFT tube was filled with brine and placed in the chamber of the spinning drop apparatus.
2. The tube was initially spun at approximately 500 rpm, and a drop of crude oil was introduced into the brine using a syringe.
3. The rotation maintained the oil drop at the center of the tube. The rotational speed was then gradually increased to 4000 rpm to ensure the drop stabilized and elongated into a spherical or cylindrical shape (**Figure 8b**).
4. During this process, the drop image was continuously captured by a high-resolution camera attached to the apparatus. The IFT values were automatically computed using the Young-Laplace equation, as shown in **Eq. 5**,

$$\sigma = \frac{\Delta d \omega^2 a^3}{2\alpha} \quad \text{.....(5)}$$

where d stands for drop diameter, m; ω is the angular frequency, rad/s; α is the cap radius, m; σ is the IFT mN/m; and α is shape parameter.

This procedure was conducted for all formulations of Moringa oleifera surfactant (MS) and MS/Silica Nanoparticles (SNPs).

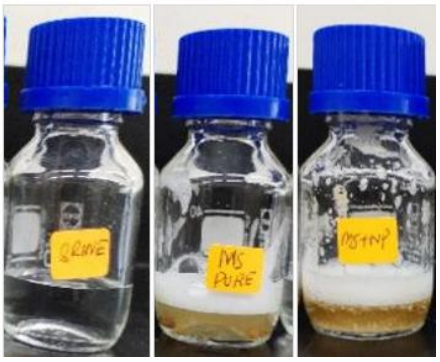

(a) Formulations for IFT & contact angle measurement

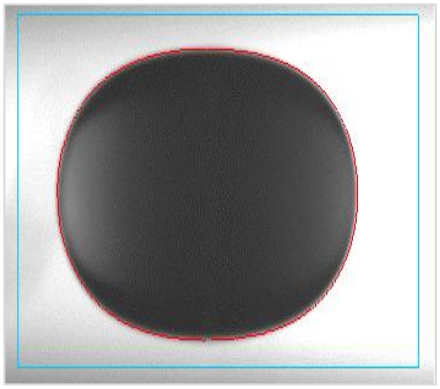

(b) Oil drop in continuous phase during IFT measurement

Figure 8—IFT measurement.

Contact Angle Measurement. The contact angle measurement was performed to assess the wetting behavior of a liquid droplet on a solid surface. This measurement provides insights into the extent to which the liquid spreads or repels on the surface. The contact angle, defined as the angle formed between the tangent lines at the liquid-solid and liquid-vapor (or liquid-air) interfaces, was determined using a drop shape analyzer. The procedure included:

1. A slice of reservoir sandstone (**Figure 9a**) was immersed in brine and each formulation separately for 48 hours to ensure full saturation of the rock (**Figure 9b**).
2. The contact angle for the oil/brine system as a control was first measured by placing the saturated sandstone on the drop shape analyzer. An oil drop was then placed on the rock surface.
3. The contact angle was recorded by measuring the tangent lines at the liquid-solid interface from both sides (**Figure 9c**).
4. This procedure was repeated for each formulation to compare the wetting behavior.

(a)Slice of reservoir rocks

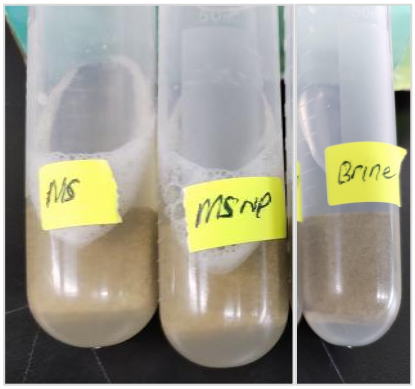

(b)Saturation of rock slice in MS, MS/SNPs and Brine solution

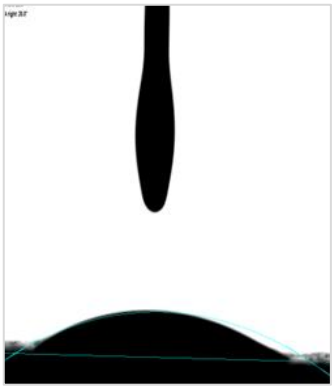

(c)Oil drop on rock surface

Figure 9—Contact angle measurement.

Results and Discussion

Physico-chemical Analysis. The physicochemical properties of Moringa oleifera oil (MO) are summarized in **Table 1**. The results reveal that the seeds yield a higher oil content (21%), attributed to the low moisture content and the chemical composition of the oil, which remains liquid at room temperature (Brontson et al. 2020). The saponification value, which indicates the number of milligrams of potassium hydroxide (KOH) required to saponify one gram of oil, suggests the suitability of MO for surfactant synthesis. This value is indicative of a lower average acid chain length (Jekayinfa and Bamgboye 2007), which is consistent with the relatively low acid number observed (Toscano et al. 2012). Consequently, the synthesis process yielded approximately 25.23 grams of surfactant.

Table 1—Physicochemical analysis results of Moringa oleifera oil (MO).

Physico-chemical parameters	Values
State at room Temp.	Liquid
Color of oil	Dark brown
Yield of oil (%)	21
Moisture content (%)	10.05
Sap. (mgKOH/g)	221.04
Acid No. (mgKOH/g)	0.16
Mass of MS (g)	25.23

The infrared spectroscopy data, presented in **Table 2**, indicates significant chemical transformations during the conversion of MO to the surfactant (MS). Specifically, the absorption peaks at 2923 and 2852 cm^{-1} observed for both MO and MS correspond to the symmetric and asymmetric stretching vibrations of CH_2 and CH_3 groups in the fatty acid chains. The peak at around 1800 cm^{-1} in MO is associated with C=O stretching, indicative of ester bonds present in triglycerides (Cleide et al. 2010). In contrast, the peak observed around 1600 cm^{-1} in MS is related to the stretching of C=C bonds, which signifies the formation of new chemical bonds during the surfactant synthesis. These peak assignments are consistent with the findings reported by Paixão et al. (2018).

Table 2—FTIR identification of functional groups in MO and MS.

Functional groups	MO FTIR (cm^{-1})	MS FTIR (cm^{-1})
C–H & CH_2 st.	2923 & 2852	2923 & 2852
-C=O st.	1800	-
-C=C st.	-	1600
-C-H bend	1500	1500
-C-O bend	1240	1100
Long chain	700	700

Adsorption Studies. In this study, a UV spectrophotometer was employed for calibration to establish a reference curve for Moringa oleifera surfactant (MS) concentrations ranging from 1-5 wt%. The calibration plot of absorbance versus concentration, shown in **Figure 10a**, yielded an R-squared value of 0.9949, indicating a high degree of correlation and validating the use of this data for subsequent adsorption studies.

Effects of MS Concentration. The experimental data from adsorption studies, depicted in **Figure 10b**, illustrate the adsorption patterns relative to MS concentrations. It is evident that an increase in MS

concentration leads to a corresponding increase in adsorption capacity. This observation highlights the significant role of surfactant concentration in influencing the adsorption efficiency. The interactions between NPs (NPs) and surfactants, crucial for the adsorption process, are mediated by electrostatic attraction, hydrogen bonding, hydrophobic interactions, and other forces (Peng et al. 2017; Zhong et al. 2019). Identifying the point of maximum adsorption is critical for optimizing performance. The maximum adsorption capacity of MS was determined to be 60.58% at a concentration of 4 wt%, indicating effective facilitation of adsorption onto NPs and a substantial surface coverage of the SNPs (Yot et al. 2014).

Effect of SNPs Dosage. **Figure 10c** illustrates the effect of SNPs dosage on adsorption capacity. The results reveal a significant impact of SNPs dosage on adsorption efficiency, with a maximum adsorption of 96% achieved at a dosage of 0.4 wt%. This enhanced adsorption is attributed to the MS molecular structure, its surface activity, and its hydrophobic/hydrophilic balance (Abooali et al. 2020).

Effect of Contact Time. The determination of equilibrium time is crucial for understanding the adsorption dynamics of MS on SNPs. As illustrated in **Figure 10d**, the adsorption of MS increases with time, reaching a maximum of 91.8% at 90 minutes. Beyond this point, further increases in contact time do not significantly impact adsorption. This equilibrium time is influenced by various factors including the nature of the adsorbate and adsorbent, temperature, pressure, and agitation conditions (Gaya 2021). Knowing the optimal contact time is essential for designing applications requiring specific adsorption levels.

Effect of Temperature. Temperature plays a significant role in both the kinetics and thermodynamics of the adsorption process. Increased temperature generally accelerates adsorption rates and can reduce the necessary contact time, although excessively high temperatures may lead to desorption of the adsorbate from the adsorbent. Conversely, lower temperatures can slow down the adsorption process or prolong the required contact time (Zheng et al. 2004). **Figure 10e** shows that the highest adsorption capacity, 81.7%, was achieved at 50°C. This indicates that moderate temperatures can enhance adsorption efficiency by optimizing the interaction between the surfactant and NPs under consistent operational conditions, including dosage, contact time, and concentration. Temperature affects the adsorption process by altering the kinetic and thermodynamic properties of surfactant-nanoparticle interactions. At moderate temperatures, reduced thermal energy can facilitate greater adherence of MS molecules to the SNPs surface (Yi et al. 2023).

Effect of pH. The impact of pH on adsorption was also investigated. The adsorption capacity of MS onto SNPs was observed to be effective at the normal basic pH of 9.41, with a peak adsorption capacity of 82.99% at pH9 (**Figure 10f**). pH affects the surface charge of NPs, which in turn influences the binding affinity of surfactant molecules (Haq et al. 2020). Adjusting pH can minimize electrostatic repulsion between surfactant molecules and NPs, enhancing adsorption through stronger attractive forces (Rattanaudom et al. 2021).

Pattamas et al. (2021) reported that surfactant solubility is often pH-dependent, and at certain pH levels, surfactants can reach their critical micelle concentration (CMC), forming micelles that are more favorable for adsorption onto NPs. Optimal pH values can stabilize the colloidal suspension of NPs, preventing agglomeration or precipitation (Manyangadze et al. 2020). Tailoring the pH can fine-tune adsorption behavior for specific applications. In this study, the objective is to achieve strong adsorption between surfactants and NPs to generate robust NPs-reinforced foams.

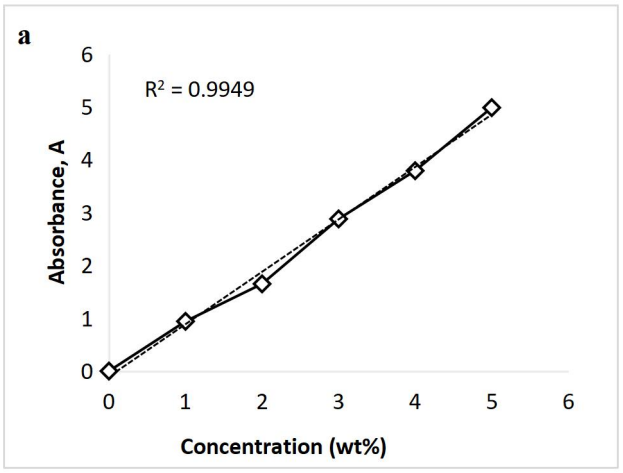

a) Calibration curve of MS concentration

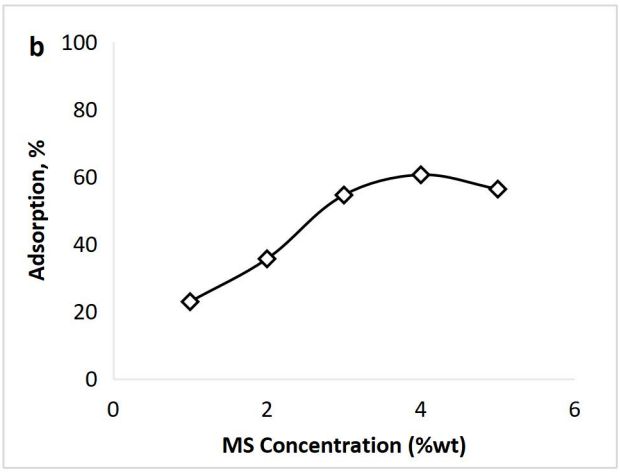

b) Effects of MS concentration

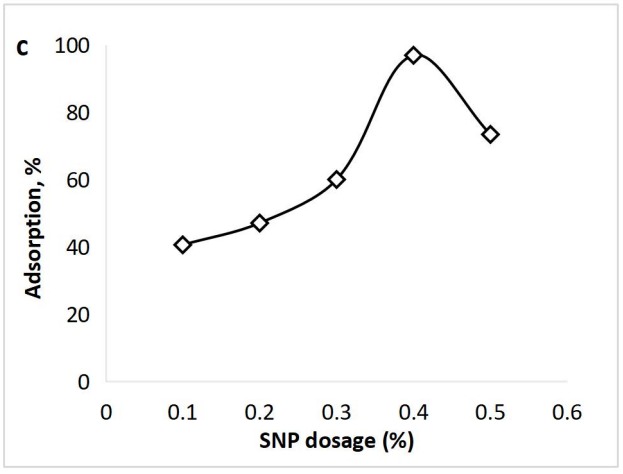

c) Effects of SNP dosage

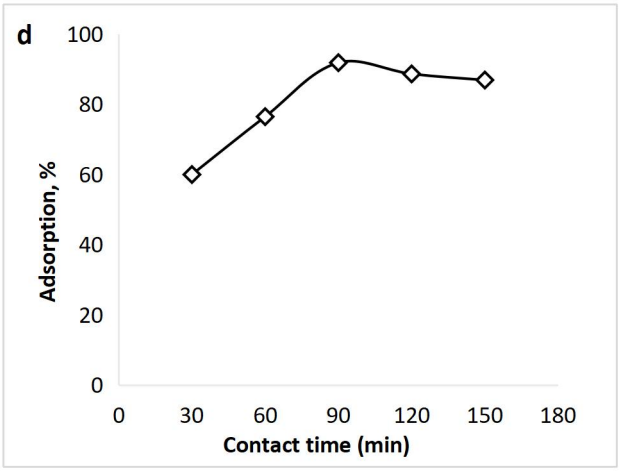

d) Effects of MS contact time

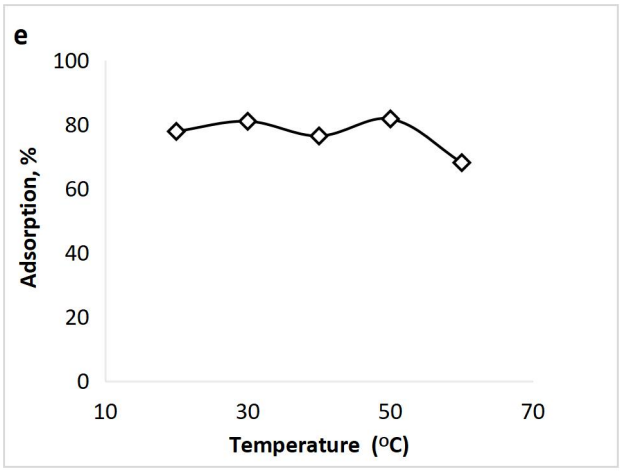

e) Effects of temperature

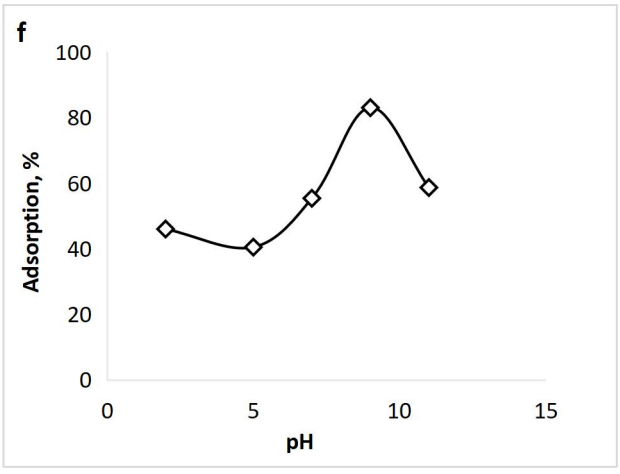

f) Effect of pH

Figure 10—Adsorption analysis result

Adsorption Isotherm Models. Adsorption isotherms are essential for designing adsorption processes as they provide insights into the relationship between the solute concentration in solution, held constant at specific pH

and temperature, and the equilibrium amount of adsorbate (MS) adsorbed onto the adsorbent (SNPs). The equilibrium data were analyzed for their fit with the Freundlich and Langmuir isotherm models.

The Langmuir isotherm model, as described by Foo and Hamid (2010), assumes the formation of a monolayer of adsorbate on the adsorbent surface. This model presupposes that all adsorption sites are energetically equivalent, and there is no interaction between adsorbed molecules, even on adjacent sites. The linearized form of the Langmuir isotherm equation is expressed as:

$$\frac{\mathrm{Ce}}{\mathrm{qe}} = \frac{1}{\mathrm{Qob}} + \frac{\mathrm{Ce}}{\mathrm{Qo}}, \quad (6)$$

Where C_e is the equilibrium concentration, mg/L; q_e is the amount adsorbed per unit weight of the adsorbent, mg/g; Q_o and b are the Langmuir constants associated with the determined maximum adsorption capacity, mg/g; and adsorption affinity coefficient, 1/mg.

This model helps in understanding the adsorption capacity and efficiency of the adsorbent by providing information about the saturation point of adsorption and the interaction between the adsorbate and adsorbent. The graph plotted between C_e/q_e *vs*. C_e, as illustrated in **Figure 11a**, can be used to determine the constants Q_o and b.

In contrast, the Freundlich isotherm model describes adsorption on a heterogeneous surface with a non-uniform distribution of adsorption sites and heat of sorption. This model is applicable to multilayer adsorption processes. The Freundlich isotherm is expressed in its logarithmic form as follows,

$$\mathrm{Log}(qe) = \log(K) + \frac{1}{n}\log(Ce), \quad (7)$$

where C_e is the equilibrium concentration of the adsorbate in solution, mg/L; K is the Freundlich constant indicative of the adsorption capacity, mg/g; n is the Freundlich exponent related to the adsorption intensity and adsorption efficiency; and q_e is the amount of adsorbate adsorbed per unit mass of adsorbent at equilibrium, mg/g.

The Freundlich model provides insight into the adsorption capacity and intensity, particularly in systems where the adsorption sites are not homogeneous and adsorption occurs in multiple layers. As seen in **Figure 11b**, the empirical constants K and ln were derived using the linear adjustments between the *log qe* and *log Ce* values. In general, the adsorption isotherms data reveal that the MS/SNPs experiment fitted better with Freundlich isotherm having R^2 of 0.9725 than the Langmuir with R^2 of 0.9052.

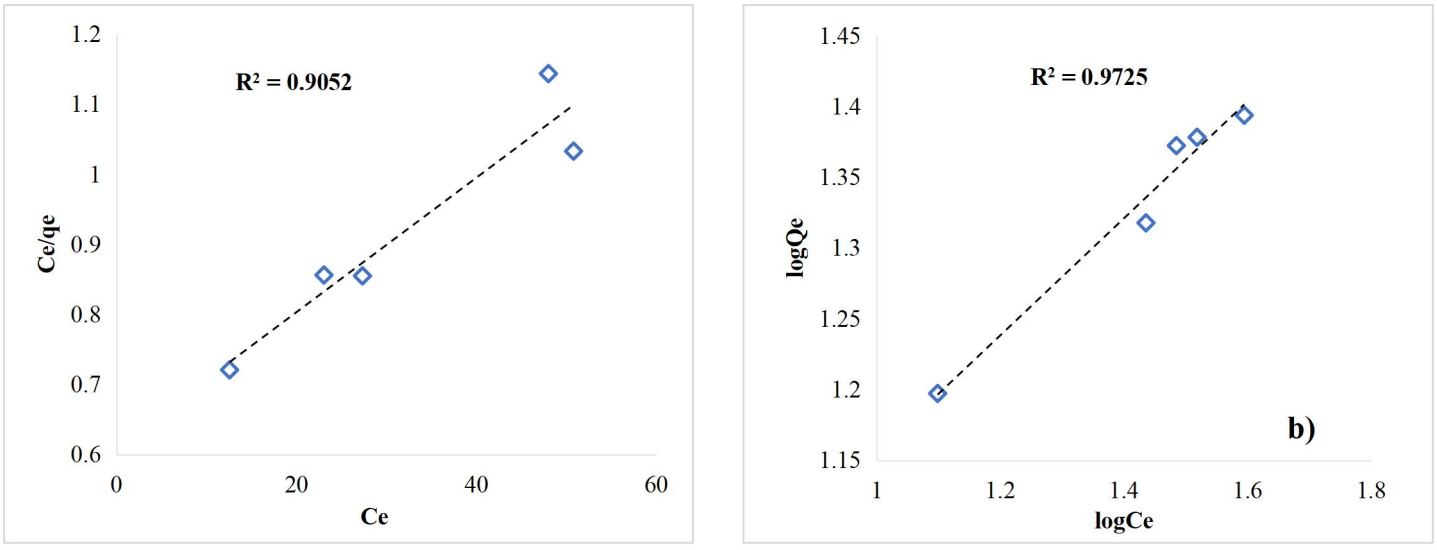

Figure 11—(a) Langmuir Isotherm and (b) Freundlich isotherm model for MS-SNPs.

Formability and Stability Analysis. The foamability results are depicted in **Figure 12a**. It is observed that the initial foam heights for both MS and MS/SNPs are similar, indicating that the presence of SNPs at a concentration of 0.4% did not significantly affect the foamability of the MS. This result suggests that the low concentration of SNPs used in this study may have been insufficient to impact foam formation significantly, which aligns with the findings of Ray et al. (2006). But this finding contrasts with several studies reporting that SNPs can influence the foamability of various surfactants (Arifur et al. 2023; Zenaida et al. 2021; Hassan et al. 2022). One possible explanation for this discrepancy could be the specific nature of the MS surfactant molecules used. Although increasing the concentration of SNPs might influence foamability, this study focused on the optimum adsorption dosage to avoid potential formation damage.

As time progresses, there is a noticeable decrease in foam heights for all samples. This decline is consistent with previous observations that brine affects initial foam heights (Abbas et al. 2024; Alireza and Delshad 2023; Hamza et al. 2022).

The foam half-life ($t_{1/2}$), defined as the time required for the foam to decompose to half of its initial volume, is shown in **Figure 12b**. Foam half-life is a key indicator of foam stability. While the exact number of degraded bubbles cannot be directly counted, foam height over time provides an indirect measure. Foam heights were normalized using the ratio of heights at time t to initial heights t_0. The foam half-lives for MS, MS/SNPs, and MS/SNPs+Brine were found to be 5, 3.2, and 3.2 minutes, respectively. A longer foam half-life generally indicates better quality and stability of the foam, which is crucial in enhanced oil recovery (EOR) foam experiments (Hamza et al. 2017).

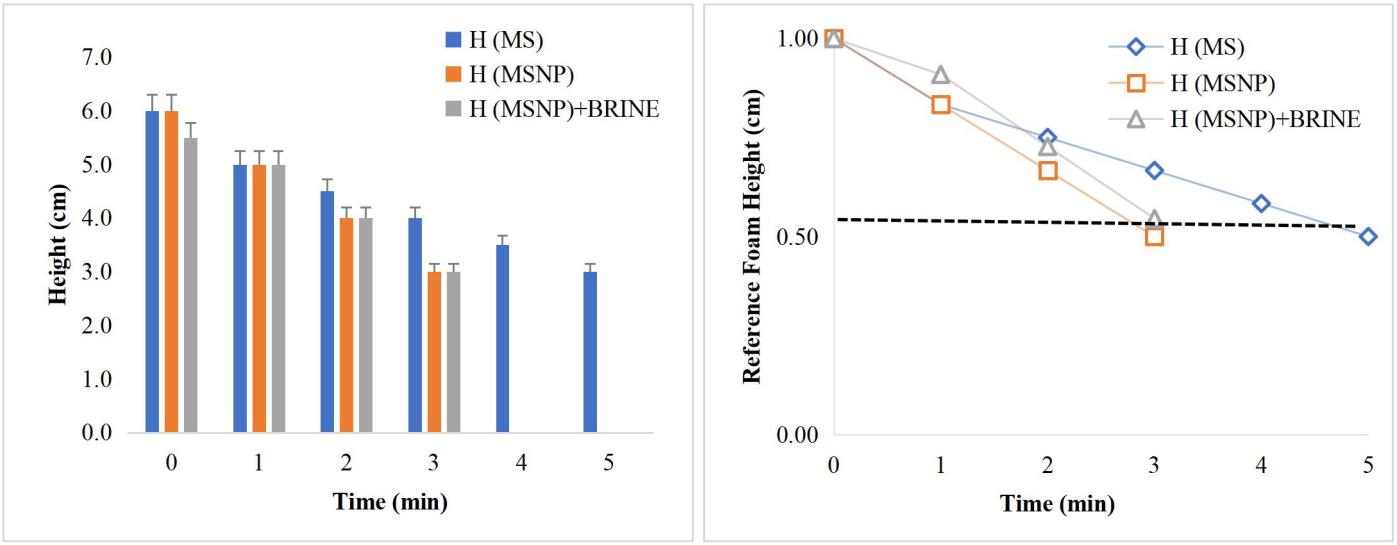

Figure 12—(a) Foamability profile and (b) foam stability.

Microscopic Analysis of Foam Bubbles. From the microscopic dimension analysis, the representative foams were examined by measuring bubble sizes and counting bubble numbers, with average foam bubble sizes presented in **Table 3**. The data indicate that the bubble size in MS foams increased linearly with time. This trend suggests that as time progresses, bubbles grow larger until they rupture and collapse due to coalescence.

In contrast, the addition of SNPs led to a decrease in bubble size. This alteration in the rheological properties of the liquid phase in the foam makes it more resistant to drainage and coarsening, thereby stabilizing the foam and preventing destabilization.

The presence of brine also affected bubble sizes, demonstrating a linear increase with time. This observation supports the impact of brine on foamability, as previously noted. Notably, a decrease in bubble size was observed with respect to MS at 0 and 5 minutes, followed by an increase.

The process of bubble coalescence can be categorized into three stages: particle collision, liquid film draining during collision, and rupture leading to larger particles. Typically, large air packets entrained in high-velocity free surface flows break into smaller bubbles and move to areas of lower shear stress, where further bubble coalescence can occur (Ummusalma and Hamza 2022).

Table 3—Foam bubble size and distribution.

TIME (min)	MS Bubble Size (cm)	Bubble Distr. (cm)	MSNP Bubble Size (cm)	Bubble Distr. (cm)	MSNP+BRINE Bubble Size(cm)	Bubble Distr. (cm)
0.00	4.66	8.20-8.89	3.84	8.60-0.80	4.17	1.48-8.49
5.00	4.68	2.59-08.08	3.95	0.85-6.20	5.23	1.48-9.05
10.00	5.33	1.04-13.89	5.42	1.19-12.49	5.37	1.67-10.87

IFT Measurements. As shown in **Table 4**, the average IFT value for the oil/brine system was measured at 6.22 mN/m. This value represents the baseline interfacial force between the oil and brine, serving as a reference point for evaluating the effects of various treatments. The introduction of MS and MS/SNPs led to significant reductions in IFT. Specifically, the IFT values dropped to an ultralow level of 0.001 mN/m for MS and 0.01 mN/m for MS/SNPs. These reductions highlight the effectiveness of the surfactant (MS) and nanoparticles (SNPs) in reducing interfacial tension.

The dramatic decrease in IFT is attributed to the surface-active properties of the surfactant and the NPs. The surfactant molecules lower the IFT by adsorbing at the oil-brine interface, while the SNPs enhance this effect through their own surface-active properties (Li et al. 2013; Hamza et al. 2018). Achieving a low IFT is crucial for successful enhanced oil recovery (EOR) operations as it facilitates the release of oil from the reservoir.

Interestingly, SNPs alone were able to maintain the IFT of MS at a nearly identical ultralow level. This result underscores the potential of combining NPs with surfactants to sustain effective IFT reduction. Several studies have explored the synergistic effects of combining NPs with surfactants to achieve significant reductions in IFT (Hamza et al. 2022; Xiao et al. 2023). The ability of SNPs to maintain such low IFT levels emphasizes their role in enhancing the performance of surfactants in EOR applications.

Table 4—Average value of IFT.

TIME (s)	BRINE (mN/m)	MS (mN/m)	MSNP (mN/m)
20	6.24	1.37×10^{-3}	1.34×10^{-3}
40	6.24	8.33×10^{-4}	4.00×10^{-7}
60	6.35	9.79×10^{-4}	1.31×10^{-3}
80	6.24	1.07×10^{-3}	1.43×10^{-3}
100	6.03	8.44×10^{-4}	2.30×10^{-6}
Average	6.22	1×10^{-3}	1×10^{-2}

Contact Angle Measurements. The illustration of some contact angle profiles for various fluids are presented in **Figure 13**. From these profiles, the average contact angle for each fluid was calculated and presented in **Table 5**. The baseline contact angle of the oil/brine system was found to be approximately $20.58\pm4.6°$, serving as a control for evaluating the effects of MS and MS/SNPs mixtures. This control fluid exhibited the highest average contact angle, indicating a relatively low wettability of the surface. This lower wettability is likely due to minimal interactions between the reference fluid and the reservoir rock, resulting in reduced spreading (Hassan et al. 2022).

In contrast, the introduction of MS and MS/SNPs led to significant reductions in the contact angle. Specifically, the contact angle decreased from 20.58±4.60° in the baseline to 16.34±2.66° for MS and further to 15.67 ± 4.06 ° for MS/SNPs. This reduction demonstrates the effectiveness of both MS and MS/SNPs in improving wettability, which is indicative of their ability to reduce interfacial tension significantly.

The observed differences in contact angle values reflect variations in wetting behavior and surface interactions with the reservoir rock (Hassan et al. 2021). Notably, the MS/SNPs mixture showed that SNPs acted synergistically with the MS surfactant, resulting in an approximate 24% reduction in IFT. This synergy corroborates the substantial adsorption capacity of the MS/SNPs system discussed earlier.

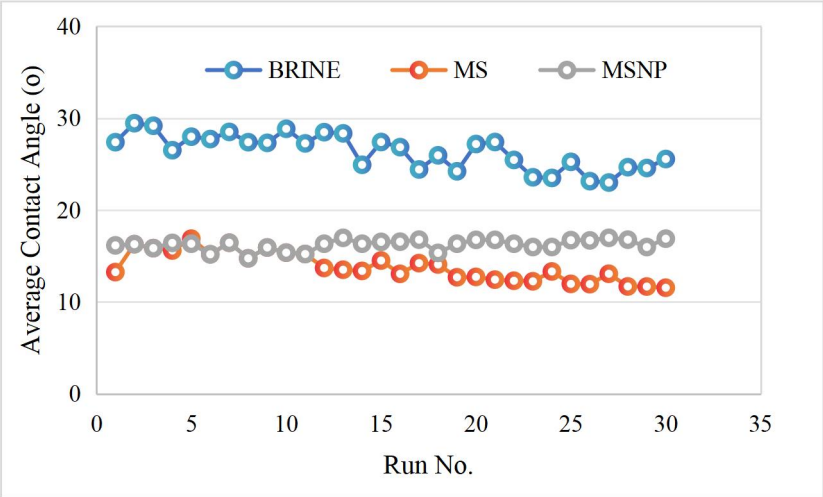

Figure 13—Contact angle profile.

Table 5—Average values of contact angle.

Fluid	Average CA (°)	% CA reduction
BRINE	20.58 ± 4.60	-
MS	16.34 ± 2.66	20
MS/SNPs	15.67 ± 4.06	24

Conclusions

This study successfully extracted essential oils from a natural source and used them to synthesize a bio-surfactant with high efficiency. Significant adsorption of MS onto SNPs was observed, attributed to Van der Waals forces and electrostatic interactions between surface charges. The optimal conditions for nanofluid adsorption were determined to be 4 wt% MS and 0.4 wt% SNPs, at a temperature of 50 °C and pH 9. These conditions align well with the Freundlich isotherm model, showing an R^2 value of 0.9725.

The foamability and stability studies demonstrated favorable results, including substantial interfacial tension (IFT) reduction and improved wettability. This novel hybrid material shows promise for enhanced oil recovery (EOR) applications, offering potential environmental benefits over traditional synthetic surfactants. Additionally, it may present economic advantages for the oil and gas industry, particularly in light of the high costs associated with treating produced water using conventional synthetic surfactants.

Further research is recommended to explore the detailed chemistry of interactions between NPs and surfactants to gain a deeper understanding of this phenomenon and optimize its applications.

Acknowledgement

The authors acknowledged Bayero University Kano, Nigeria, Universiti Teknologi MARA, Malaysia and Universiti Teknologi Petronas, Malaysia.

Nomenclature

A = Volume of KOH solution;
B = Blank ;
b = Adsorption affinity coefficient, 1/mg;
C_e = Equilibrium concentration, mg/L;
C_i = Initial concentration, wt% or mg/L;
C_f = Final concentration, wt% or mg/L;
CA = Contact angle, ^{o};
CEOR = Chemical Enhanced Oil Recovery;
CMC = Critical Micellar Concentration;
D = Drop diameter, m;
EOR = Enhanced oil recovery;
FTIR = Fourier transform infrared spectroscopy;
IFT = Interfacial tension;
K = Freundlich constant;
KOH = Potassium hydroxide;
M = Mass, g;
M = Molarity, mol/L;
M_1 = Initial mass, g;
M_2 = Final mass, g;
Mbpd = Millions barrel per day;
MS = Moringa Oleifera surfactant;
MO = Moringa Oleifera oil;
N = Normality, eq/L;
n = Freundlich exponent;
NPs = Nanoparticles;
OOIP = Original oil in-place;
Q_e = Amount adsorbed per unit weight of the adsorbent, mg/g;
Q_o = Langmuir constants ;
SNPs = Silica nanoparticles;
S = Sample;
$t_{1/2}$ = Half-life;
UV = Ultra Violet;
V = Volume, mL;
w = Weight, g;
H = Foam height, cm;
σ = IFT, mN/m;
ω = Angular frequency, rad/s;
ɑ = Cap radius, m;
α = Shape parameter, m;

Competing interests

The author(s) declare that they have no conflicting interests.

References

Abbas, K.M., Mahboobeh, M., Jagar, A., et al. 2024. Performance Evaluation of the Green Surfactant-Treated Nanofluid in Enhanced Oil Recovery: Dill-Hop Extracts and SiO_2/Bentonite Nanocomposites. *Energy & Fuels* **38**(3):1799-1812.

Abooali, D., Soleimani, R., and Gholamreza-Ravi, S. 2020. Characterization of Physico-Chemical Properties of Biodiesel Components Using Smart Data Mining Approaches. *Fuel* **266**(1): 117075.

Ahmadi, M. A. and Shadizadeh, S.R. 2013. Induced Effect of Adding Nano Silica on Adsorption of a Natural Surfactant onto Sandstone Rock: Experimental and Theoretical Study. *Journal of Petroleum Science and Engineering* **112**(1): 239-247.

Ali, A., Yusof, Y.A., Chin, N.L., et al. 2017. Processing of Moringa Leaves As Natural Source of Nutrients by Optimization of Drying And Grinding Mechanism. *Journal of Food Process Engineering* **40**(1): 12583

Alireza, B. and Delshad, M. 2023. Strategy for Optimum Chemical Enhanced Oil Recovery Field Operation. *Journal Resource Recovery* **1**(1): 100-120.

Aljuboori, F.A., Lee, J. H., Elraies, K. A., et al. 2019. Gravity Drainage Mechanism in Naturally Fractured Carbonate Reservoirs-Review and Application. *Energies* **12**(19):3699.

Arifur, R., Farshid, T., and Ezeddin, S. 2023. Surfactant and Nanoparticle Synergy toward Improved Foam Stability. *Petroleum* **9**(2): 255-264.

Asante, W.J., Nasare, D., Tom-Dery, K., et al. 2014. Nutrient Composition of Moringa Oleifera Leaves from Two Agro Ecological Zones in Ghana. *African J. Plant.* **8**(1): 65-71.

Atta, D.Y, Negash, B.M, and Yekeen, N. A. 2021. A State-of-theart Review on the Application of Natural Surfactants in Enhanced Oil Recovery. *Journal of Molecular Liquids* **321**(1):114888.

Ray, G.B., Chakraborty, I., and Moulik, S.P. 2006. Pyrene Absorption Can Be a Convenient Method for Probing Critical Micellar Concentration (CMC) and Indexing Micellar Polarity. *Journal of Colloid and Interface Science* 294(1):248-254.

Blaker, T., Aarra, M.G., Skauge, A., et al. 2002. Foam for Gas Mobility Control in the Snorre Field: The FAWAG Project. *SPE Res Eval & Eng* **5**(4): 317-323. SPE-78824-PA.

Cleide, S.T., Araújo, E.I., Melo, V.N., et al. 2010. Moringa Oleifera Lam. Seeds as a Natural Solid Adsorbent for Removal of Ag in Aqueous Solutions Adsorption Contraction Mechanics. *J. Braz. Chem. Soc.* **21**(9): 1727-1732.

Emilianny, R., Batista, M., Nadja, N.F., et al. 2021. Effect of Oil Extraction on the Composition, Structure, and Coagulant Effect of Moringa Oleifera Seeds. *Journal of Cleaner Production* **279**(1):123902.

Rattanaudom, P., Shiau, B. J., Suriyapraphadilok, U., et al. 2021. Effect of pH on Silica Nanoparticle-Stabilized Foam For Enhanced Oil Recovery Using Carboxylate-Based Extended Surfactants. *Journal of Petroleum Science and Engineering* **196**(1):107729.

Freer, E.M., Svitova, T.F., and Radke, C.J. 2003. The role of interfacial rheology in reservoir mixed wettability, Journal of petroleum Science and Engineering. 39: 137-158.

Foo, K and Hameed, B. 2010. Insights into the modeling of adsorption isotherm systems. Chemical Engineering Journal. 156:2-10.

Gaya, U. 2021. Recent Approaches, Catalysts and Formulations for Enhanced Recovery of Heavy Crude Oil. Journal of Periodica Polytechnica Chemical Engineering, 65(4), pp. 462–475.

Hamza, M.F., Sinnathambi, C.M., and Merican, Z. M. A. 2016. Recent Advancement of Hybrid Materials Used in Chemical Enhanced Oil Recovery (CEOR): A Review. *IOP Conf. Series: Materials Science and Engineering* **206**(1):35-60.

Hamza, M.F., Sinnathambi, C.M., Merican, Z. M. A., et al. 2017. An Overview of the Present Stability and Performance of EOR-foam. *Sains Malaysiana* **46**(9):1641-1650.

Hamza, M.F., Sinnathambi C.M., Merican, Z. M. A., et al. 2018. Effect of SiO_2 on the Foamability, Thermal Stability and Interfacial Tension of a Novel Nano-Fluid Hybrid Surfactant. *International Journal of Advanced and Applied Sciences* **5**(1): 113-122.

Hamza, M.F.,Soleimani, H., Merican, Z. M. A., et al. 2020. Nano- fluid Viscosity Screening and Study of In-situ Foam Pressure Buildup at High- Temperature High- Pressure Conditions. *Journal of Petroleum Exploration and Production Technology* **10**(1):1115-1126.

Hamza, M.F., Soleimani, H., Ridha, S., Abdelazim, A., Sikiru, S., 2022. Double Layer Chemical Encapsulation of SiO_2 Nanoparticles for Interfacial Tension Reduction under Low Salinity Condition. *Journal of Molecular Liquids* **371**(1):121100.

Haq, B., Al Shehri, D., Al Damegh, A., et al. 2020. The Role of Carbon Nanotubes (CNTs) and Carbon Particles in Green Enhanced Oil Recovery (GEOR) for Arabian Crude Oil in Sandstone Core. *The APPEA Journal* **60**(1):133-145.

Hassan, Y.M., Guan, B.H., Zaid, H.M., et al. 2021. Application of Magnetic and Dielectric Nanofluids for Electromagnetic-Assistance Enhanced Oil Recovery: A Review. *Crystals* **11**(1):106.

Hassan, Y.M., Guan, B.H., Chuan, L.K., et al. 2022. The Influence of ZnO/SiO2 Nanocomposite Concentration on Rheology, Interfacial Tension, and Wettability for Enhanced Oil Recovery. *Chem. Eng. Res. Des.* **179**(1):452-461.

Jekayinfa, S.O. and Bamgboye, A.I. 2007. Development of Equations for Estimating Energy Requirements in Palm-Kernel Oil Processing Operations. *Journal of Food Engineering* **79**(1):322-329.

Joshi, S.J., Geetha, S.J., Desai, A.J. 2015. Characterization and Application of Biosurfactant Produced by Bacillus licheniformis. *Appl. Biochem. Biotechnol.* **177**(1):346-361.

Kamal, M.S., Hussein, I.A., Sultan, A.S. 2017. Review on Surfactant Flooding: Phase Behavior, Retention, IFT, and Field Applications. *Energy Fuels* **31**(1):7701-7720.

Kalibbala, H.M., Wahlberg, O., and Hawumba, T.J. 2009. The Impact of Moringa oleifera as a Coagulant Aid on the Removal of Trihalomethane (THM) Precursors and Iron from Drinking Water. *Water Science and Technology: Water Supply* **9**(6):707-714.

Lakshmipriya, G., Kruthi, D., and Devarai, S.K. 2016. A Review on Nutritive Importance and Its Medicinal Application. *Journal of Science Direct, Food Science and Human Wellness* **5**(1):549-560.

Li, S., Hendraningrat, L., and Torsaeter, O. 2013. Improved Oil Recovery by Hydrophilic Silica Nanoparticles Suspension. Paper presented at the International Petroleum Technology Conference, Beijing, China, 26-28 March. IPTC-16707-MS.

Manyangadze, N. H. M., Chikuruwo, T. B., Narsaiah, C.S., et al. 2020. Enhancing Adsorption Capacity of Nano-Adsorbents via Surface Modification: A Review. *South African Journal of Chemical Engineering* **31**(1):25-32.

Nguyen, T.P., Hesemann, P., and Hankari, S.E. 2014. Precursor Mediated Synthesis of Nanostructured Silicas: From Precursor-Surfactant Ion Pairs to Structured Materials. *Journal of Materials* **7**(4):2978-3001.

Osama, M. and Ahmad S. A. 2020. The Use of Surfactants in Enhanced Oil Recovery: A Review of Recent Advances. *Energy Reports* **6**(1):3150-3178.

Oyeyinka, A.T. and Oyeyinka, S.A. 2018. Moringa oleifera as a Food Fortificant: Recent Trends and Prospects. *Journal of the Saudi Society of Agricultural Sciences* **17**(2):127-136.

Pattamas, R., Bor-Jier, S., Uthaiporn, S., et al. 2021. Tuning Contact Angles of Aqueous Droplets on Hydrophilic and Hydrophobic Surfaces by Surfactants. *J. Phys. Chem. B* **126**(1):3374-3384.

Paixão, R.M., Reck, I.M., Gomes, R.G., et al. 2018. Water Decontamination Containing Nitrate Using Biosorption with Moringa oleifera in Dynamic Mode. *Environ Sci Pollut Res* **25**(1):21544-21554.

Peng, C., Min, F., and Liu, L. 2017. Effect of pH on the Adsorption of Dodecylamine on Montmorillonite: Insights from Experiments and Molecular Dynamics Simulations. *Appl. Surf. Sci.* **425**(1):996–1005.

Hou, Q., Zhu, Y., Luo, Y., et al. 2012. Studies on Foam Flooding EOR Technique for Daging Reservoirs After Polymer Flooding. Paper presented at the SPE Improved Oil Recovery Symposium, Tulsa, Oklahoma, USA, 14-16 April. SPE-151955-MS

Salehi, M.M., Sahraei, E., Nejad, S.A. 2014. Comparison of Oil Removal in Surfactant Alternating Gas with Water Alternating Gas, Water Flooding and Gas Flooding in Secondary Oil Recovery Process. *J. Petrol. Sci. Eng.* **120**(1):86-93.

Toscano, G., Riva, G., Foppa Pedretti, E., et al. 2012. Vegetable Oil and Fat Viscosity Forecast Models Based on Iodine Number and Saponification Number. *Biomass Bioenergy* **46**(1):511-516.

Ummusalma, S.M. and Hamza, M.F. 2022. Fenugreek Surfactant: Extraction, Synthesis and Evaluation of Foam Properties for Application in Enhanced Oil Recovery. *Applied Science and Technology Express* **2022**:1-9**.**

Xiao, D., Muhammad, S.K., Shirish, P., et al. 2023. Investigation of the Coupled Effect of IFT Reduction and Wettability Alteration for Oil Recovery. *ACS Omega* **8**(13):12069-12078.

Yarima, M.H., Beh, H.G., Lee, K.C., et al. 2022. The Influence of ZnO/SiO_2 Nanocomposite Concentration on Rheology, Interfacial Tension, and Wettability for Enhanced Oil Recovery. *Chemical Engineering Research and Design* **179**(1):452-461.

Yekeen, N., Eswaran, P., Kamal, I., et al. 2019. Surfactant Adsorption Behaviors onto Shale from Malaysian Formations: Influence of Silicon Dioxide Nanoparticles, Surfactant Type, Temperature, Salinity and Shale Lithology. *Journal of Petroleum Science and Engineering* **179**(1):841-854.

Yi, L., Zheng, Z., Hao, G.P., et al. 2023. Fine Tuning CO_2 Adsorption and Diffusion Behaviors in Ultra-Microporous Carbons for Favorable CO_2 Capture at Moderate Temperature. *Journal of Sustainable Chemistry for Climate Action* **2**(1):100015.

Yot, P.G., Boudene, Z., Macia, J., et al. 2014. Effect of Temperature on the Adsorption of Organic Vapors on Activated Carbon Fibers. *Chemical Communications* **50**(1):9462-9464.

Zenaida, B.A., Soltero-M., J.F.A., et al. 2021. Aqueous Foams and Emulsions Stabilized by Mixtures of Silica Nanoparticles and Surfactants. *Chemical Engineering Journal Advances* **7**(1):100116.

Zhang, J., Gao, H., and Xue, Q. 2020. Potential Applications of Microbial Enhanced Oil Recovery to Heavy Oil. *Crit. Rev. Biotechnol.* **40**(1):459-474.

Zhao, G., Dai, C., Zhang, Y., et al. 2015. Enhanced Foam Stability by Adding Comb Polymer Gel for In-Depth Profile Control in High Temperature Reservoirs. *Journal of Physicochemical and Eng. Aspects* **482**(1):115-124.

Zheng, H., Huang, F.K., and Jiming, H. 2004. Effect of Contact Time Adsorption of Rhodamine B, Methyl Orange and Methylene Blue Colors on Langsat Shell with Batch Methods. *J. Phys.: Conf. Ser.* **1788**(1):012008.

Zhong, X., Li, C., Pu, H., et al. 2019. Increased Nonionic Surfactant Efficiency in Oil Recovery by Integrating with Hydrophilic Silica Nanoparticle. *Energy Fuels* **33**(1):8522-8529.

Umar Hassan is an Assistant quality assurance/control officer at Dangote Petroleum Refinery and Petrochemical (DPRP), Nigeria. He holds BSc. (Hons.) in Industrial Chemistry from Bayero University Kano, Nigeria, in 2017, and currently a registered postgraduate (MSc) student of Physical Chemistry (awaiting viva) in the Department of Pure & Industrial Chemistry, Bayero University Kano, Nigeria. His research revolves around exploring the potential of nanotechnology for enhanced oil recovery.

Dr. **Mohammed Falalu Hamza** is a senior lecturer in the School of Chemistry & Environment, Universiti Teknologi MARA (UiTM), Malaysia. Prior to joining UiTM in 2024, Dr. Falalu has worked for about 11 years at the Department of Pure & Industrial Chemistry, Bayero University Kano (BUK), Nigeria. Dr. Falalu's research focuses in Nano chemistry with applications in Enhanced Oil Recovery (EOR), surfactant formulation, foam generation, nanoparticles modification, transport phenomena and formation damage. He holds B.Sc. (Hons.) in Industrial Chemistry from BUK, Nigeria, in 2009, MSc in Chemistry from University of KwaZulu Natal, South Africa, in 2014, PhD in Applied Sciences from Universiti Teknologi Petronas (UTP), Malaysia, in 2019, and Postdoctoral research at Institute of Hydrocarbon Recovery, UTP, Malaysia, in 2023.

Dr. **Hassan Soleimani** is an Associate professor of Physics (Wave Propagation), Universiti Teknologi PETRONAS where he has been working as a faculty member for 16 years. His research interests are in Nanotechnology, Electromagnetism, Materials Science, Optics and Geophysics. Dr. Hassan holds BSc. (Hons.) in Physics from University of Isfahan, Iran in 1992, MSc. in Physics from Bahonar Kerman University, Kerman, Iran in 1997, and PhD in Physics from University Putra Malaysia (UPM), Malaysia in 2010. Dr. Soleimani has served as a visiting scientist at University of Cambridge, UK (2012), Wright State University, USA (2013), University of Patras, Greece (2014), and Griffith University, Australia (2015).

Dr. **Bashir Abubakar Abdulkadir** is a postdoctoral fellow with the Centre for Research in Advanced Fluid & Processes, Universiti Malaysia Pahang. He holds B.Sc. (Hons.) in Chemistry from Gombe State University (GSU), Nigeria in 2010, MSc. and PhD in Chemistry from Universiti Teknologi Petronas, Malaysia in 2015 and 2022, respectively. He has been a lecturer at GSU, Nigeria and actively undertake research in polymer electrolytes as energy sources, catalysts and catalysis for hydrogen storage and production.

Dr. **Saifullahi Imam Shehu** is a lecturer and researcher in the Department of Pure and Industrial Chemistry, Bayero University Kano (BUK), Nigeria. He holds PhD in Surface Chemistry and Catalysis from Universiti

Sains Malaysia, in 2020, MSc in Physical Chemistry from SRM University, India in 2015, and BSc. (Hons) in Chemistry from BUK, Nigeria in 2010. His research interests are in environmental remediation, photocatalysis, fenton reactions, conversion of wastes to wealth and adsorption.

Dr. **Sabiha Hanim Saleh** is an Associate Professor Chemistry & Environment in the School of Chemistry & Environment, Universiti Teknologi MARA (UiTM), Malaysia. Her research interests are in Industrial Waste Utilization and Green Chemistry. Dr. Saleh holds PhD in Environmental Health & Waste Management from Universiti Sains Malaysia (USM) in 2010, MSc. in Environment from Universiti Putra Malaysia (UPM) in 1999, BSc. (Hons.) in Chemistry from Universiti Kebangsaan Malaysia (UKM) in 1996, and Diploma in Science, Institut Teknologi MARA (ITM) in 1992.